

Astrophysical Tests of Modified Gravity: Constraints from Distance Indicators in the Nearby Universe

Bhuvnesh Jain¹, Vinu Vikram¹, Jeremy Sakstein²

ABSTRACT

We use distance measurements in the nearby universe to carry out new tests of gravity, surpassing other astrophysical tests by over two orders of magnitude for chameleon theories. The three nearby distance indicators – cepheids, tip of the red giant branch (TRGB) stars, and water masers – operate in gravitational fields of widely different strengths. This enables tests of scalar-tensor gravity theories because they are screened from enhanced forces to different extents. Inferred distances from cepheids and TRGB stars are altered in opposite directions over a range of chameleon gravity theory parameters, well below the sensitivity of cosmological probes. Using published data we have compared cepheid and TRGB distances in a sample of unscreened dwarf galaxies within 10 Mpc. As a control sample we use a comparable set of screened galaxies. We find no evidence for the order unity force enhancements expected in these theories. Using a two-parameter description of the models (the coupling strength and background field value) we obtain constraints on chameleon theories as well as symmetron and dilaton screening scenarios. In particular we show that $f(R)$ models with background field values f_{R0} above 5×10^{-7} are ruled out at the 95% confidence level. We also compare TRGB and maser distances to the galaxy NGC 4258 as a second test for larger field values. While there are several approximations and caveats in our study, our analysis demonstrates the power of gravity tests in the local universe. We discuss the prospects for additional, improved tests with future observations.

1. Introduction

1.1. Modified Gravity

Modified theories of gravity (MG) have received a lot of attention in recent years. Several unexplained phenomena such as the observed accelerated expansion of the universe, spatio-temporal variation of the fundamental constants (e.g. the fine-structure constant) and dark matter can in principle be explained by modifying general relativity (GR) on large (astrophysical and greater) scales. This study is motivated by recent work on MG to obtain cosmic acceleration without

¹Department of Physics & Astronomy, University of Pennsylvania, Philadelphia, PA 19104, USA

²Department of Applied Mathematics and Theoretical Physics, Cambridge, CB3 0WA, UK

invoking quintessence-like dark energy. Even on theoretical grounds, GR is unlikely to be the complete theory of gravity owing to singularities and its non-renormalizability. Hence it is generally considered to be the low energy effective action of some UV-complete theory (though our interest is modifications in the long distance/low energy regime).

Any modification to GR generically introduces an additional degree of freedom (Weinberg 1965) and scalar-tensor theories, where a new scalar field couples non-minimally to gravity, are ubiquitous in many attempts to find consistent theories. Theories such as DGP (Dvali, Gabadadze & Porrati 2000) invoke braneworld scenarios that contain large extra dimensions and appears as a scalar-tensor theory to observers in four dimensions. The low energy effective action of string theory contains a new scalar particle, the dilaton, coupled non-minimally to gravity and any theory with $\mathcal{N} = 4$ supergravity (or higher) contains at least two scalar fields in the gravity multiplet. Even attempts to modify the geometrical properties of GR tend to lead to scalar-tensor theories; for example the entire class of $f(R)$ theories is equivalent to a single scalar field coupled non-minimally to matter via a Weyl rescaling of the metric.

Thus a wide class of gravity theories contain a coupling of the scalar field to matter via a universal fifth force which leads to enhancements of the gravitational force. Non-relativistic matter – such as the stars, gas, and dust in galaxies – will feel this enhanced force and as a consequence, a general feature of scalar-tensor theories is that dynamically inferred masses are larger than the true masses. The discrepancy can be up to a factor of 1/3 in $f(R)$ or DGP gravity (for recent reviews see Silvestri & Trodden (2009) and Jain & Khoury (2010)). Photons do not feel the enhanced force, so that lensing probes the true mass distribution.

This enhanced gravitational force should be detectable through fifth force searches such as the Eöt-Wash experiment (Kapner et al. 2007) and Casimir force experiments (e.g. Decca et al 2003) as well as tests of the equivalence principle (Mota & Shaw 2006)¹ or through the orbits of planets around the Sun (Will 2006). However, since all of these experiments have been performed in our local vicinity, i.e. the solar system, they do not rule out any large-scale modifications where fifth forces are active over large (cosmological) scales while matching the predictions of GR within experimental bounds on small scales. Any theory where the fifth forces are suppressed on small scales is said to possess a *screening mechanism*: regions where fifth forces are active are said to be *unscreened* whereas those where they are suppressed are *screened*. Khoury & Weltman (2004) proposed such a mechanism where non-linear screening of the scalar field, known as *chameleon screening*, can suppress the fifth force in high density environments such as the Milky Way, so that solar system and laboratory tests can be satisfied.

In this paper we will consider deviations from GR exhibited in theories that rely on chameleon screening. Qualitatively similar behaviour occurs in symmetron screening (Hinterbichler & Khoury

¹If the scalar coupling to matter is not constant then one generically expects violations of the weak equivalence principle.

2010) and the environmentally dependent dilaton (Brax et al. 2010) and the tests we will present here apply to these mechanisms as well. We also note that chameleon screening was originally suggested to hide the effects of a quintessence-like scalar that forms the dark energy and may couple to matter (generically such a coupling is expected unless forbidden by a symmetry). Hence there are reasons to expect such a screening effect to operate in either a dark energy or modified gravity scenario, or even in scenarios that don't relate to cosmic acceleration such as the scalar fields invoked in string theories.

A different screening mechanism, Vainshtein screening (Vainshtein 1972), operates by including non-canonical kinetic terms in the field equations whose non-linear nature acts to recover GR on scales smaller than some *Vainshtein radius*. In theories that contain this mechanism (such as DGP, massive gravity and Galileons) this radius must typically be taken to be of the order of the length scale of typical galaxies, independent of their mass, and so does not produce the observable effects considered here (see Appleby and Linder 2012 for recent cosmological constraints for a subclass of Galileon theories). However recent studies have pointed out the possibility of enhanced forces even within galaxies in Vainshtein theories, opening them up to astrophysical tests (Chan & Scoccimarro 2009; Hui & Nicolis 2012).

1.2. Observations of the Nearby Universe

The logic of screening of the fifth force in scalar-tensor gravity theories implies that signatures of modified gravity will exist where gravity is weak. In particular, dwarf galaxies in low-density environments may remain unscreened as the Newtonian potential Φ_N , which determines the level of screening, is at least an order of magnitude smaller than in the Milky Way. Hence dwarf galaxies can exhibit manifestations of modified forces in both their infall motions and internal dynamics. Hui, Nicolis & Stubbs (2009) and Jain & Vanderplas (2011) discuss various observational effects while Vikram et al (2012, in preparation) present a set of tests from current observations.

Stars within unscreened galaxies may show the effects of modified gravity. Chang & Hui (2010) and Davis et al. (2011a) describe the effects on giant and main sequence stars, respectively: essentially the enhanced gravitational force makes stars of a given mass brighter and hotter than in GR. They are also more ephemeral since they consume their fuel at a faster rate. For the Sun the potential $\Phi_N \approx 2 \times 10^{-6}$ (we set $c = 1$ and work with the amplitude of the potential throughout). Coincidentally, the potential of the Milky Way is close to this value – and is believed to be sufficient to screen the galaxy so that solar system tests of gravity are satisfied². Thus main sequence stars whose masses are similar to that of the Sun are likely to be partially or completely screened. It is worth noting that these screening conditions are found by considering static, non-dynamical

²At least this is the straightforward interpretation; there may be loopholes to this logic where the galaxy is screened by the Newtonian potential of the local group or structure on larger scales

spherical objects sitting inside a fixed scalar field. Davis et al. (2011a) have shown that stars, as dynamical objects which support themselves under the action of the enhanced gravity, can be partially unscreened at Newtonian potentials where this simple model would predict them to be completely screened, especially for higher mass objects.

Red giants are at least ten times larger in size than the main sequence star from which they originated so they have $\Phi_N \sim 10^{-7}$ – thus their envelopes may be unscreened. The enhanced forces lead to smaller radii, hotter surface temperatures and higher luminosities than their GR doppelgangers. For $f(R)$ theories with background field values (f_{R0}) in the range 10^{-6} – 10^{-7} , Chang & Hui (henceforth CH) find that compared to GR a solar mass red giant has radius R smaller by over 5%, luminosity L larger by over 50% at fixed effective temperature T_e , while T_e itself is higher by about 5% at fixed L . They point out that the change in surface temperature of about 150 Kelvin may be detectable from data on the red giant branch in observed Hertzsprung-Russel (HR) diagrams.

We focus on specific stages of the evolution of giants and supergiants to seek different observational signatures. The first feature, well known for its use in obtaining distances, is the nearly universal luminosity of $\lesssim 2M_\odot$ stars at the tip of the red giant branch. The second is the Period-Luminosity relation of cepheids, which are giant stars with $\sim 3 - 10M_\odot$ that pulsate when their evolutionary tracks cross a near universal, narrow range in T_e known as the *instability strip*. The tight relation between luminosity and other observables is what makes these stars valuable distance indicators – it also makes them useful for tests of gravity. For background field values in the range 10^{-6} – 10^{-7} , the TRGB luminosity is largely robust to modified gravity while the cepheid $P - L$ relation is altered. Measurements of these properties within screened and unscreened galaxies then provide tests of gravity: the two distance indicators should agree for screened galaxies but not for unscreened galaxies.

This paper is organized as follows: In §2 we briefly describe chameleon gravity (a full discussion for the interested reader is given in Appendix A) and explain the differences in stellar evolution due to its influence. In §3 the properties of cepheids in GR and MG are presented, as well as a summary of relevant observations; the corresponding details of TRGB distances are presented in §4. §5 contains our main results based on a comparison of cepheid and TRGB distances. Water masers in NGC 4258 are used for a second tests in §6, and other distance indicators are discussed. We conclude in §7.

2. Modified Gravity and its Effect on Stellar Structure

2.1. Review of Chameleon Screening

Here we will briefly review the parameters that provide tests of gravity, motivated by the chameleon-like screening mechanisms. We refer the interested reader to Appendix A for the full

details and examples of some of the more common models.

There are two parameters in these theories. The first, χ_c (see Appendix A and Davis et al. 2011a) determines how efficient the body is at screening itself. If the magnitude of the surface Newtonian potential $\Phi_N \ll \chi_c$ then the object will be completely unscreened whilst if the converse is true then the body will be at least partially screened (see equation A9 in appendix A). Currently there are two different constraints on χ_c in the literature. The Newtonian potential of the Sun is around 2×10^{-6} and the Milky way has a similar value and so if one demands that these objects self screen then $\chi_c \gtrsim 10^{-6}$ is ruled out observationally. Independent constraints come from cosmological observables and cluster abundances and set an upper bound $\chi_c \approx 10^{-4}$ for $f(R)$ models (Schmidt, Vikhlinin & Hu 2009; Lombriser et al 2010 and references therein). Our analysis here constitute an independent constraint, so we examine several possible uses of TRGB, cepheid and water maser distance indicators to test gravity.

The second parameter in these models is α_c , which sets the strength of the fifth force in unscreened regions. A completely unscreened object will feel a fifth force that is proportional to the Newtonian force and the combined forces simply amount to a rescaling of G by

$$G \rightarrow G(1 + \alpha_c). \quad (1)$$

For partially screened objects, the total force in the region exterior to the screening radius can be described by a position dependent rescaling of G :

$$G(r) = G \left[1 + \alpha_c \left(1 - \frac{M(r_s)}{M(r)} \right) \right] \quad (2)$$

where $M(r)$ is the mass interior to a shell of radius r .

We will consider tests of chameleon theories that probe ranges of χ_c and α_c well below current astrophysical limits. For concreteness in evaluating screening conditions we work with $f(R)$ models, which are chameleon models with parameters:

$$\alpha_c = 1/3; \quad \chi_c = f_{R0}. \quad (3)$$

where f_{R0} is a parameter commonly used in the literature to constrain the model (Hu & Sawicki 2007). $\alpha_c = 1/3$ is also the value found in the high density limit of the environmentally dependent dilaton (see Appendix A). We will also consider other values of α_c in comparisons with observations.

In $f(R)$ theories, the parameter f_{R0} sets the screening condition for an isolated spherical halo (Hu & Sawicki 2007): $\Phi_N > \frac{3}{2}f_{R0}$. The Navarro-Frenk-White (NFW) density profile is a good approximation for halos of most galaxies both in GR and $f(R)$ theories (Lombriser et al. 2012). It is useful to express the Newtonian potential in terms of the scale radius r_s of the NFW profile as:

$$\Phi_N^{NFW} = \frac{GM_g}{r} \ln(1 + r/r_s) \quad (4)$$

where we have followed Hu & Sawicki (2007) in using M_g to represent the mass contained within $5.3r_s$ (see also Schmidt 2010). The screening condition can then be conveniently expressed in terms of the observable maximum circular velocity v_{\max} as:

$$\left(\frac{v_{\max}}{100 \text{ km/s}}\right)^2 \gtrsim \frac{f_{R0}}{2 \times 10^{-7}}. \quad (5)$$

For the late-type dwarf galaxies of interest here, the peak circular velocity is likely to be reasonably well estimated by the observed rotation curves. The effects of inclination and of limited radial coverage typically lead to 10% level underestimates of v_{\max} . For the range of circular velocities used in our sample, we probe f_{R0} values in the range $10^{-6} - 10^{-7}$.

2.2. Stellar Structure and Evolution

The structure of a spherically symmetric star is obtained by solving the equations of stellar structure that at a given radius r relate $M(r)$ to $P(r)$, $\rho(r)$ and $T(r)$ – respectively the pressure, density and temperature. The opacity κ and the energy generation rate ϵ are needed to close the equations. We will denote the radius of the star as R , so that $M = M(R)$ is the total mass and $L = L(R)$ the total luminosity. P , κ and ϵ are determined in terms of ρ and T by equations of state which are independent of gravitational physics. As noted by CH and Davis et al. 2011a, modifying gravity only alters the gravitational physics, which is entirely contained in the equation of hydrostatic equilibrium:

$$\frac{dP}{dr} = -\frac{G(r)\rho(r)M(r)}{r^2}, \quad (6)$$

which represents the condition for the outward pressure to balance the (now enhanced) inward gravitational pull and remain static. Note that the modification is expressed purely as a change in G , which becomes dependent on r if the star is partially screened according to equation 2. The other three equations – the continuity, radiative transfer and energy generation equations – are all unaffected by this change in G . The result is that unscreened stars of a given mass are more compact, brighter, and have a larger effective temperature than screened stars of identical mass and chemical composition. They also have a shorter main sequence life-time due to their increased burning rate and finite fuel supply.

We will assume that changes in the gravity theories occur on timescales longer than the evolutionary timescales of stars. Since we are interested in massive post-main sequence stars, evolutionary timescales are shorter than a billion years, typically orders of magnitude smaller. Thus provided the main sequence is the same as in GR (i.e. for $f_{R0} < 10^{-6}$), the star’s post-main sequence evolution begins at the same point in the HR diagram as in GR, and subsequently responds to a static (but possibly r -dependent) G . Our results do not require this assumption but it simplifies the story.

The complete system of stellar structure equations for main sequence stars can be solved under certain simplifying assumptions (see Davis et al. 2011a). However, if one really wants to

look at the dynamical and nuclear properties, as well as the structure of post main sequence stars then a numerical prescription is needed. In this work we shall use a modification of the publicly available stellar evolution code MESA (Paxton et al. 2011) presented in (Davis et al. 2011a). MESA can simulate individual stars of any given initial mass and metallicity and includes a fully consistent implementation of nuclear reaction networks, mass loss, convection, radiative transfer, opacity tables and metallicity effects. In brief, it is a one-dimensional (in that it assumes spherical symmetry) code that divides the star into radial cells of unequal width, each with a set of properties such as mass, temperature etc. The implementation of chameleon gravity into MESA uses a quasi-static approximation where the structure of the star is solved first and then the value of G is updated in every cell given this structure. This approximation is good provided that the time between successive stellar models is smaller than the timescale over which the changes in $G(r)$ are significant and MESA provides a facility to ensure that this is always the case. This method has been checked against that used by CH, who use a scalar-field ansatz and interpolation between different cells, and the results have been found to be indistinguishable. Our method uses the general screening properties set out in Appendix A and as such, applies to generic screening behavior, not only chameleons.

The implicit relation for the screening radius is given in appendix A (equation A9) and is completely equivalent to the condition

$$\chi_c = 4\pi G \int_{r_s}^R r \rho(r) dr. \quad (7)$$

Given an initial stellar model, the integral 7 is performed from the stellar surface, cell by cell until the condition is satisfied. The cell where this is so is then designated as the screening radius and the value of G is changed according to equation 2 in all cells exterior to this. The star is then allowed to evolve under this new gravity until the next stellar model is reached and the process is repeated.

3. Cepheid Variables

3.1. Cepheid Pulsations in GR

Cepheids are a class of massive, pulsating giant stars whose time period P is related to luminosity L in a well understood way. After a giant reaches the tip of the red giant branch, its luminosity falls and it moves into the core Helium burning stage. Stars that are sufficiently massive, $M \gtrsim 3M_\odot$, actually follow trajectories called loops, which at three or more phases cross the instability strip – set by a narrow range in effective temperature T_e . While in the instability strip, their luminosity and radius oscillate with a time period of days-weeks in a very regular manner. We are concerned here with a class of pulsating stars called (classical) cepheids. The radial oscillations in a cepheid are the result of acoustic waves resonating within the star. For much of the lifetime

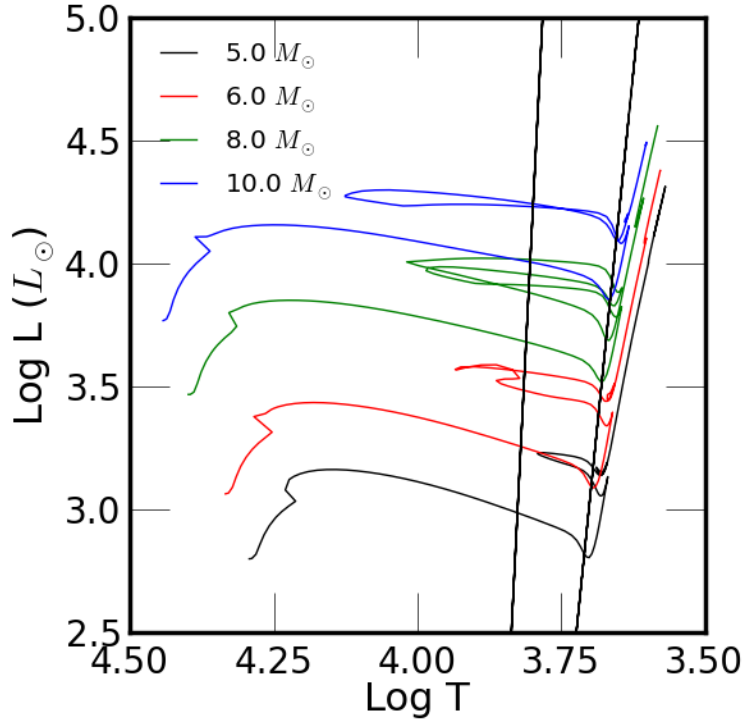


Fig. 1.— The post-main sequence HR diagram (L vs. T_e) is shown for stars with different masses as indicated. The black vertical lines shows the blue edge (left) and red edge (right) of the instability strip. At each crossing of the instability strip the star pulsates as a cepheid variable. The fits for the instability strip are taken from Alibert et al 1999.

of a star, its envelope is stable to pulsations – the exception is the instability strip. Figure 1 shows the post main sequence evolution of stars of different masses.

The instability strip arises due to the presence of a He^+ ionization zone in the stellar envelope located where the temperature is around 4×10^4 K (corresponding to the ionization potential of He). The pulsation is driven by the κ -mechanism (and to a small extent the γ -mechanism³). The opacity throughout the majority of the star is given by Kramer’s law, $\kappa(R) \propto \rho T^{-3.5}$. In the ionization zone however, the gradient $d \ln \kappa / d \ln T \gg -3.5$ and so a small compression, which increases the temperature slightly, causes a large increase in the opacity, absorbing radiation and damming up energy. This further increases the opacity, resulting in an outward pressure which drives the pulsations. This driving is only really effective when the thermal time-scale of the zone is comparable to the pulsation period, which requires it to be located in the so called *transition region*, where the stellar processes (which are adiabatic in the star’s interior) are becoming non-

³This is where the energy absorbed from the radiation is used to ionize the He and not to raise the temperature and so small compressions raise the opacity by virtue of the increased density, the opposite of their usual effect.

adiabatic. The instability strip therefore corresponds to the region in the H-R diagram where the ionization zone coincides with this transition region.

Stars can cross the instability strip multiple times. The 1st crossing of the instability strip is before the star goes up the red giant branch and is far too brief to be observationally irrelevant. The 2nd crossing of the instability strip is the first crossing after the tip of the red giant branch when the star is on the lower part of the blue loop. And the 3rd crossing is when it is on the upper part of the blue loop. The 2nd and 3rd crossing of the strip, and in particular on the blue edge, is probably where cepheid properties are best understood. There are nearly as many observed cepheids on the 2nd and 3rd crossing. We will use the 3rd crossing of a 6 solar mass star as our fiducial case (observed cepheids are typically 6-8 solar mass stars).

To estimate the pulsation period, one needs to go beyond hydrostatic equilibrium and consider the full dynamical radial acceleration of a fluid element at radius r , which is described by the momentum equation:

$$\ddot{r} = -\frac{GM(r)}{r} - \frac{1}{\rho} \frac{\partial P}{\partial r} \quad (8)$$

The time period of pulsations Π may be estimated through various approximations: 1. As the sound crossing time for the diameter of the star, giving $\Pi \propto 1/\sqrt{\gamma G \rho}$ where γ is the ratio of specific heats and ρ is the mean density of the star. This expression assumes that physical variables like the density and temperature can be used. The dependence on G and ρ is essentially correct, but the dependence on γ is not correct. 2. By perturbing equation 8 as well as the equations of continuity, radiative transfer and energy generation one can derive a full non-adiabatic wave equation for infinitesimal fluid elements in the Lagrangian picture (see Cox 1980). If one linearises this equation in the adiabatic limit and searches for standing wave solutions then the resultant eigenvalue equation for the radial wave, the linear adiabatic wave equation (LAWE), gives the pulsation periods. The LAWE is highly non-trivial and depends on the zeroth order pressure and first adiabatic index Γ_1 and so the general case requires numerical matrix or shooting methods applied to simulations involving envelope models. One simplifying assumption that can be made however is that of a static sphere of fixed equilibrium radius and constant density composed of gas with an adiabatic relation $\delta P/P \propto \gamma \delta \rho/\rho$. Under this assumption, the LAWE can be solved for the period of small oscillations (note that the linear and adiabatic nature precludes a calculation of the amplitude) to find:

$$\Pi = \frac{2\pi}{\sqrt{4/3\pi G \rho (3\gamma - 4)}}. \quad (9)$$

Using $\gamma = 5/3$ for an ideal monatomic gas yields $\Pi = \sqrt{3\pi/G\rho}$ Π above is in the range of 1-100 days for a range of relevant red giant densities. This equation gives values of Π that are fairly close to more detailed calculations as well as observations.

We note that detailed numerical models are able to predict not just the period but many detailed properties of cepheids, including the variations of size and luminosity, the location of the instability strip, and the dependence on mass and metallicity (e.g. Bono et al 1998). The primary

source of uncertainty is the treatment of convection, so to some extent input from observations is used in theoretical models.

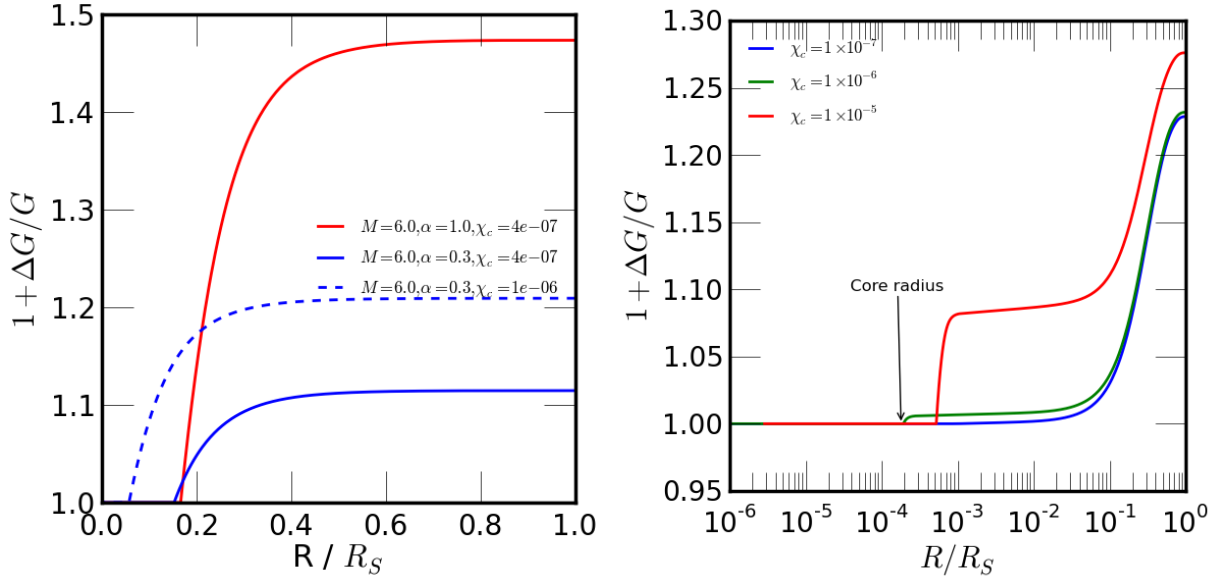


Fig. 2.— The profile of the effective gravitational constant G inside the star for cepheids (left panel) and TRGB stars (right panel). Note that cepheid pulsations typically span $0.3 < R/R_S < 0.9$ while the core physics that sets the TRGB luminosity occurs deep within the star. The core radius in the right panel is shown by the arrow for $\chi_c = 10^{-5}$. The plateau just below 1.1 on the y-axis shows the enhanced gravity in the H-burning shell.

3.2. Cepheid Pulsations in Modified Gravity

The effect of MG theories on cepheid pulsations is well approximated by considering the deviation of G from its Newtonian value G_N . We apply Eqn. 9 to estimate the change in period for two choices of a constant G : in an idealized, completely unscreened star the first corresponds to the coupling constant $\alpha_c = 1$, and the second to $\alpha_c = 1/3$, which applies to all $f(R)$ models (see above). The modified gravitational constant is denoted G_1 and G_2 for the two cases, and the corresponding periods Π_1 and Π_2 are:

$$G_1 = 2 G_N \implies \Pi_1 = \Pi_N / \sqrt{2} \quad (10)$$

$$G_2 = 4/3 G_N \implies \Pi_2 = \Pi_N / \sqrt{4/3} \quad (11)$$

where the subscript N denotes values in the Newtonian gravity. The shorter period means that in chameleon gravity, the inferred distance (based on incorrectly using the GR Period-Luminosity relation) is smaller than the true distance.

A fully unscreened star is an idealization – it is important to take into account the spatial profile of G and the fact it is not altered inside the screening radius. This will tend to lower the deviation. We take this into account and estimate a more realistic value of ΔG in the unscreened region by averaging $G(r)$ according to

$$\langle G \rangle = \frac{1}{R} \int_0^R f(r)G(r) dr \quad (12)$$

where $G(r)$ is given by equation 2. The function $f(r)$ is a weighting function that accounts for the fact that different regions of the star are more important than others in driving the pulsations. The simplest scenario is to simply take $f(r) = 1$, however Epstein (1950) has numerically solved the pulsation equation and tabulated the weight function f (see figures 1 and 2 in his paper). Using the numerical values given in the tables, we have reconstructed the normalized weight function. We use the Epstein function in conjunction with $G(r)$ profiles from MESA along the instability strip to obtain $\langle G \rangle$. Figure 2 shows the actual profiles $G(r)$ for different choices of α_c and χ_c .

To estimate the change in distance, we need the Period-Luminosity relation for a given observational band. If one uses $\rho \sim M/R^3$ in Equation 9, and $L = 4\pi R^2 \sigma T_e^4$, then one gets a relation between Π , L and T_e that is nearly universal for all cepheids. The main residual dependence is on metallicity. Using observational quantities, such as the V-band absolute magnitude M_V (note though that it is the bolometric magnitude M_B that is directly related to L) and (intrinsic) color $B - V \propto \log T_e$ gives

$$M_V = \tilde{\alpha} \log \Pi + \tilde{\beta}(B - V) + \tilde{\gamma} \quad (13)$$

where $\tilde{\alpha}$ and $\tilde{\beta}$ are universal in galaxies with similar metallicity, e.g. the Milky Way and other galaxies dominated by Pop II stars. For the observations discussed below a reasonable approximation is $\tilde{\alpha} \approx -3$. Using the $P - L$ relation above and the fact that the flux goes as L/d^2 , the change in inferred distance is

$$\frac{\Delta d}{d} \approx -0.3 \frac{\Delta G}{G}, \quad \text{where} \quad \frac{\Delta G}{G} \equiv \frac{\langle G \rangle - G_N}{G_N}. \quad (14)$$

Table 1 gives the effective values of $\Delta G/G$ obtained from MESA and the resulting change in distance⁴.

Note that we test for gravity using these predicted changes in distance using a sample of galaxies each of which has dozens to hundreds of observed cepheids. While systematic errors in absolute distances are a challenge, as is theoretical uncertainty, we use relative distances in our tests, so some gain in accuracy is achieved via averaging over many cepheids and galaxies.

The above estimates are based on simple approximations for the theory of cepheid pulsations. We do not address the amplitude of the oscillations, which depends on luminosity and other

⁴The absolute value of $\tilde{\alpha}$ is significantly larger in the infrared, which would lead to larger changes in distance. It also provides an additional check on gravity: the inferred distance should vary with filter. We estimate a change in distance of about 5% between the V and K band.

Table 1: Change in inferred distance due to the change in cepheid periods for different gravity parameters. For a $6M_{\odot}$ cepheid, the change in effective G (using the Epstein weights as described in the text) and inferred distance is shown for different values of the coupling constant α_c and background field value χ_c . All $f(R)$ models correspond to $\alpha_c = 1/3$ with $\chi_c \equiv f_{R0}$.

α_c	χ_c	$\Delta G/G$	$\Delta d/d$
1/3	4×10^{-7}	0.11	-0.03
1/3	1×10^{-6}	0.21	-0.06
1/2	4×10^{-7}	0.17	-0.05
1/2	1×10^{-6}	0.34	-0.09
1	2×10^{-7}	0.21	-0.06
1	4×10^{-7}	0.45	-0.12

properties. Nor does our analysis deal with the location of the instability strip which involves the Luminosity-Mass-effective Temperature relation; the instability strip itself is quite narrow, $\simeq 200\text{K}$. The amplitude and shape of the pulsations, the precise value of the period, as well as location of the instability strip are reasonably well understood and well measured. Changes in these properties are therefore additional possible tests of gravity. The computation involves the use of detailed non-linear, non-adiabatic models that are well studied in the literature (though the treatment of convection and metallicity dependence remain somewhat uncertain). For MG, this also requires modeling the evolution up to the instability strip via MESA. These issues are beyond the scope of this study and will be addressed elsewhere.

We use only the distances obtained from the $P - L$ relation for our tests below: it is worth noting that our analysis is robust to the effects of MG on the luminosity and radius of the star. To see this note that in obtaining a distance estimate from the $P - L$ relation of Eqn. 13, the observables are the flux f , T_e and Π while the coefficients $\tilde{\alpha}$ and $\tilde{\beta}$ follow from $L = 4\pi\sigma R^2 T_e^4$. So the entire dependence on MG is via G ; the change in G may be regarded as contained in the coefficient γ . In practice $\tilde{\alpha}$ and $\tilde{\beta}$ are set empirically since observations involve filters with finite wavelength coverage, so estimates of the flux and temperature are imperfect. We have used the empirical value $\tilde{\alpha} \approx -3$ to check that the residual dependence on L is weak: $\Delta d/d \approx -0.025\Delta L/L$ at constant T_e – at least a factor of ten smaller than the signal from MG models we consider. An additional effect is the mass dependence of MG effects (more massive stars have slightly larger force enhancements). This leads to shallower predicted slopes of the $P - L$ relation and other second order effects that we do not consider here but merit further study.

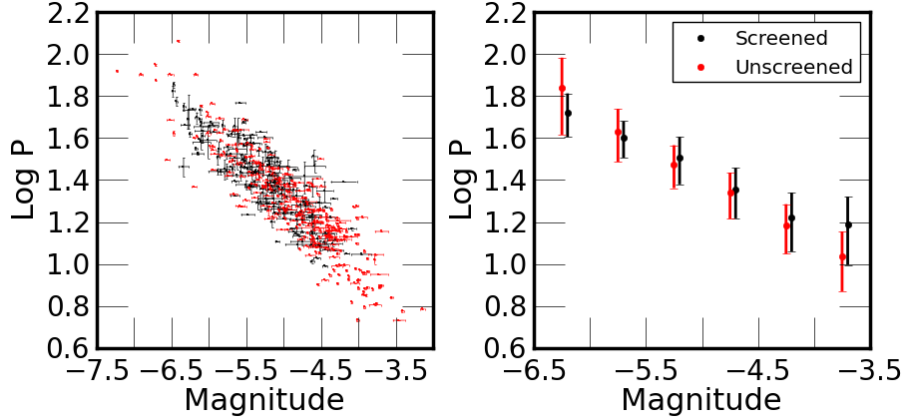


Fig. 3.— The $P - L$ relation for the galaxies in our sample. In the left panel, we show all the cepheids observed along with the reported error bars. The right panel shows the mean period and dispersion within bins in absolute magnitude of size 0.5. The red and black points show unscreened and screened galaxies respectively. There is no evidence for a difference in the shape of the $P - L$ relation between the two samples.

3.3. Observations of Cepheids

Cepheid distances have been calibrated using parallaxes for 10 Milky Way cepheids in the distance range $\approx 0.3 - 0.6$ kpc, with periods ranging from $\approx 3 - 30$ days. The error on the mean distance is $\pm 3\%$ or 0.06 magnitude. The slope has in the past been obtained from the LMC since the sample size is bigger, but at the cost of possible uncertainty due to metallicity effects. More recently the maser distance to NGC 4258 has superseded the calibration with the LMC. Outside the Local Group, cepheid distances have been measured to over 50 galaxies (see the review by Freedman & Madore 2010 for more details). The final uncertainty in the distance modulus, which includes zero point calibration, metallicity, reddening and other effects, is ± 0.09 magnitude or 5% in distance.⁵ As discussed in Sasselov et al (1997) and subsequent work, the three basic ingredients in the $P - L$ relation (pulsation theory, stellar evolution and stellar atmospheres) are sensitive to metallicity. A metal-poor cepheid is fainter for given period and temperature. The net dependence on metallicity however is weak, in particular the slope of the relation between period and bolometric luminosity is nearly unchanged.

The data for the $P - L$ relation used in our analysis was compiled for individual cepheids in 19 galaxies – see Appendix C for details. Five galaxies were removed from the sample due to the large

⁵The *GAIA* space telescope will improve cepheid calibration. An important recent development is the measurement of the $P - L - C$ relation in the IR. The slope is steeper and the scatter is significantly smaller in the IR, so *Spitzer* and *JWST* should improve the calibration. A factor of two improvement is anticipated – see Table 2 in Freedman & Madore (2010).

scatter in the relation. Of the remaining 14 galaxies used for Figure 3, seven galaxies have TRGB based distances as well. The majority of the galaxies show late type morphology and include both dwarf and normal galaxies with peak rotational velocities ranging from 40 to 240 km/s. The number of cepheids in each galaxy varies between 5 and 117, and is in the range 10-50 for most galaxies. We use only cepheids with good photometry in V-band. We use the phase-weighted cepheid luminosity when possible (available for the majority of the cepheids) and intensity-weighted luminosity for the remainder. Compiling this dataset requires a detailed compilation of data on hundreds of cepheids, so we have used only a subset of existing data. The sample size can be significantly increased to carry out additional tests, given more detailed theoretical predictions for MG as discussed below.

We classify these galaxies as screened or unscreened based on their mass (which determines whether the self-screening condition is satisfied) and their environment. No rigorous criteria exist to determine the screening effect of the neighboring galaxies, groups and clusters since the equations are nonlinear. However, based on recent work (Zhao et al 2011; Cabre et al 2012) and on tests we have performed, we use an estimate of the mean Newtonian potential over the galaxy due to its neighbours within a (background) Compton wavelength. This is estimated from the SDSS, 2MASS and other surveys, and used to determine the screening condition in combination with Eqn. 5 for self-screening (details are presented in Cabre et al 2012).

Figure 3 shows the observed $P - L$ relation in our sample. We use the normalization from Saha et al (2006) to find the absolute magnitude. The left panel shows the individual data points with error bars and the right panels shows the averaged $P - L$ relation in bins of absolute magnitude. The red points show cepheids in unscreened galaxies and black points in screened galaxies. The slope of the $P - L$ relation is consistent between the two samples. The unscreened sample has a slightly steeper slope – we have checked that the expected signal from MG is the opposite, based on changes in the period which is shorter for massive cepheids. We do not use this signature as a test here since there are uncertainties in the model predictions. However, this is a potential future test for MG.

4. TRGB: Tip of the Red Giant Branch Distances

The TRGB distance is obtained by comparing the measured flux to the universal peak luminosity expected for red giants with masses below $2 M_{\odot}$. TRGB distances have been measured to ~ 250 galaxies using the universality of the peak luminosity of red giants at the tip of the red giant branch. These are applied to old, metal poor populations which enables distance estimates out to about 20 Mpc, a bit closer than cepheid distances since cepheids are brighter. However since single epoch photometry suffices, it is much easier to obtain the data for a TRGB distance. While it is not an absolute distance method, and must in fact be calibrated using secondary indicators like cepheids, a comparison of TRGB distances in screened and unscreened galaxies can still provide a useful test.

Table 2: Change in inferred distance using the TRGB peak luminosity for different gravity parameters. For a $1.5M_{\odot}$ red giant, the change in luminosity and the inferred distance is shown for different values of the coupling constant α_c and background field value χ_c . All $f(R)$ models correspond to $\alpha_c = 1/3$ with $\chi_c \equiv f_{R0}$.

α_c	χ_c	$\log L/L_{\odot}$	$\Delta d/d$
0	0	3.34	0
1/3	1×10^{-6}	3.32	0.02
1/3	2×10^{-6}	3.30	0.04
1/3	4×10^{-6}	3.25	0.12
1/3	8×10^{-6}	<3	>0.20

The TRGB luminosity is set by the He flash during the post main sequence evolution. Low mass stars develop a small He core region after the main sequence (which grows slower than that of high mass stars). In the initial stage of post-main sequence evolution the core temperature is not high enough to ignite the He and the core subsequently contracts due to the absence of outward pressure. This catalyses the nuclear reaction in the outer hydrogen dominated region and the He produced in the shell gets deposited on to the core. The increase in the mass of the core causes the shell luminosity to grow – for stars of interest the luminosity of the star is roughly $\propto M_c^{23/3}/R_c^6$, where M_c and R_c are the mass and radius of the core. When the core temperature becomes high enough ($T_c \sim 10^8 K$) to ignite He, the star moves to the left in the H-R diagram, settling onto the horizontal branch. Nuclear physics within the core sets the TRGB luminosity, mostly independent of composition or mass of the envelope.

The luminosity of the TRGB depends on the mass of the core which in turn depends weakly on the metallicity of the star. In particular, for stars with low metallicities ($-2.2 \leq [\text{Fe}/\text{H}] \leq -0.7$) the I band magnitude of the TRGB varies by only 0.1 magnitude within this metallicity range ($I_{TRGB} = -4.0 \pm 0.1$), though it can vary a lot more in other bands. Figure 1 in Lee, Freeman & Madore (1993) shows the variation of M_V and M_I over the above metallicity range. The remarkable constancy of the TRGB magnitude leads to a discontinuity in the luminosity function of stars as low mass stars continuously reach this phase. The distance to the TRGB can be measured if we can filter out the magnitude at the discontinuity. Observationally, the TRGB is identified from a semi-empirically calibrated color-magnitude diagram (Da Costa & Armandroff 1990) and the metallicity corrected distance modulus is determined.

We have estimated the change in luminosity with modified gravity for the TRGB using MESA (see Appendix B for a discussion and an analytic estimate). Figure 2 shows the profiles of $G(r)$ at the TRGB stage for a $1.5M_{\odot}$ star for different values of χ_c with $\alpha_c = 1/3$. There is a transition in the enhancement of G inside the core as χ_c increases from 10^{-6} to 10^{-5} . We find that for $\alpha = 1/3$, the resulting change in luminosity is at the percent level for $\chi_c < 10^{-6}$. However for χ_c between

$5 \times 10^{-6} - 10^{-5}$, the shell becomes unscreened and the luminosity changes rapidly, falling by 20% to over 50% in this range. The change in distance that would result is detectable – a fact used in the comparison of TRGB and maser distances below. Table 2 gives the change in inferred distance $\Delta d/d$ for different values of χ_c .

The TRGB data used here is taken from the literature and involves many telescopes, including WFPC2/ACS on board the Hubble Space Telescope, the 5m Hale telescope at Palomar Observatory, Isaac Newton Telescope Wide Field Camera, Wisconsin Indiana Yale NOAO 3.5m telescope, VLT etc. The photometry on these images was done using the DAOPHOT and/or ALLFRAME (Stetson 1987, 1994) packages. The observed magnitudes are corrected for foreground extinction. Methods like Sobel edge-detection (Lee, Freeman & Madore 1993), maximum likelihood (Méndez et al. 2002) etc. were used to estimate the TRGB magnitude. We classify the galaxies into screened and unscreened samples as for the cepheids.

5. Results: Constraints on Gravity Theories with Cepheid and TRGB Distances

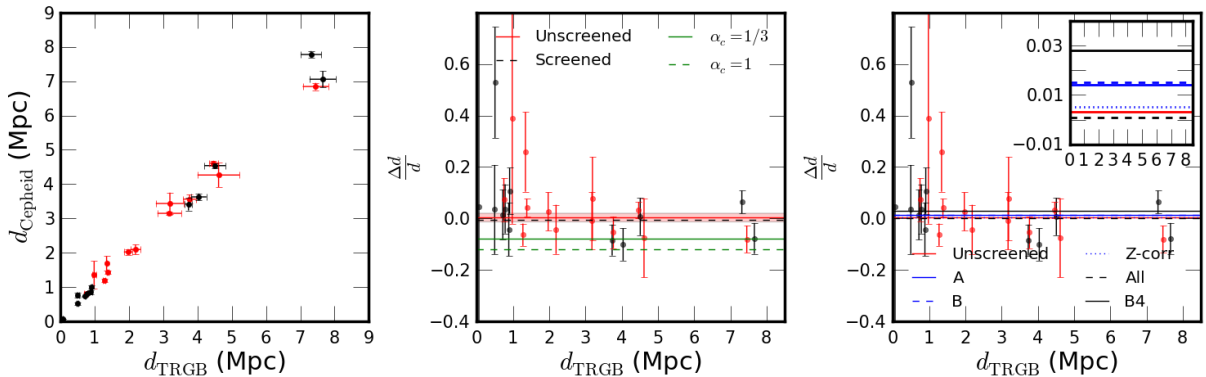


Fig. 4.— *Left panel:* A comparison of distances measured using the cepheid $P - L$ relation and TRGB luminosities. The black points are for screened galaxies and the red points for unscreened galaxies. *Middle panel:* $\Delta d/d$, the fractional difference between cepheid and TRGB distances, as a function of TRGB distance. The shaded region in the middle panel shows the 68% confidence region around our best fit to the unscreened sample (red line). The best fit to the screened sample is shown by the dashed black line. The data are consistent with the GR expectation of zero deviation in distance and there is no visible trend in the deviation with whether the galaxy is screened or not. The dotted and dashed green lines show two possible predictions of chameleon theories with $\alpha_c = 1$, $\chi_c = 4 \times 10^{-7}$ and $\alpha_c = 1/3$, $\chi_c = 1 \times 10^{-6}$ which corresponds to $f(R)$ gravity. *Right panel:* As checks on systematic errors and model uncertainties, the four lines show the best fits obtained with other choices for the screening threshold or metallicity correction – see text for details. These lines lie within the 68% confidence region shown in the middle panel.

We began with a sample of 27 galaxies with both TRGB and cepheid distances taken from

Table 3: Best fit values for $\Delta d/d$ and uncertainty σ in the fractional difference between cepheid and TRGB distances, for screened and unscreened subsamples. Our estimated σ includes systematic errors; the number of galaxies N and reduced χ^2 is also given.

Sample	N	$\Delta d/d$	σ	Reduced χ^2
Unscreened	13	0.003	0.017	1.0
Screened	12	-0.005	0.022	1.3

the literature compiled by Madore & Steer using NED⁶. This sample includes 12 galaxies from the Hubble Space Telescope Key Project (Freedman et al. 2001). Other galaxies in their sample do not have TRGB distance measurements. For many galaxies more than one measurement exists both for TRGB and cepheid based distances. We use bootstrap resampling to obtain the average and error bars on those measurements. We exclude one galaxy with TRGB distance beyond 10 Mpc and another galaxy (DDO 187) which has only two confirmed cepheids. This leaves us with 25 viable galaxies.

We perform a likelihood analysis on the data to estimate the best fit value of $\Delta d/d$. The best values and 1- σ errors are given in Table 3 along with the reduced χ^2 . We included empirically estimated systematic errors in the estimate of the distance to each galaxy from multiple measurements, as well as in the average deviation $\Delta d/d$ for each subsample of galaxies. For the latter we made the ansatz that each galaxy has an additional unknown systematic error that can be added in quadrature to the reported error. By further assuming that the systematic error was the same for each galaxy, we could estimate σ_{sys} iteratively such that the reduced χ^2 was unity. We found that the systematic error thus estimated is subdominant for the majority of galaxies.

We have tested our estimate of statistical and systematic errors by using several different methods of weighting the multiple distance measurements for each galaxy, of outlier rejection and bootstrap resampling. The various estimates lie within the 1- σ interval shown and generally tend to deviate towards positive values (i.e. further away from the MG predictions; see below). Note that for higher values of χ_c the TRGB distances are also affected in a way that increases Δd : the inferred distance would be larger in modified gravity since the peak luminosity is lower. So the predicted deviation from cepheid distances increases for $\chi_c \gtrsim 10^{-6}$.

Figure 4 shows the cepheid distance vs. the TRGB distance for this sample of galaxies, separated into screened (black points) and unscreened (red points) subsamples. The middle and right panels show $\Delta d/d$, the fractional difference between the cepheid and TRGB distances. The shaded region in the middle panel shows the 68% confidence region around our best fit (red line) for the unscreened sample. The dashed black line shows the best fit for the screened sample – it nearly

⁶<http://ned.ipac.caltech.edu/level5/NED1D/ned1d.html>

overlaps the red line. Clearly the screened and unscreened samples are consistent. The two green lines show the predictions for chameleon theories with coupling strength $\alpha_c = 1/3, 1$ and values of χ_c as indicated. The two models shown are ruled out at over 95% confidence.

In the right panel of Figure 4 we show some alternate estimates of $\Delta d/d$. Since our estimate of the Newtonian potential due to neighbors is subject to uncertainties in the galaxy catalog, we show two other screening criteria, labeled A and B, with threshold $\Phi_N = 2 \times 10^{-7}$ and 1×10^{-6} (our fiducial choice is 4×10^{-7}). We also show the result obtained using the full sample of galaxies (labelled All). The three best fits are within the 68% confidence region of the middle panel, in fact they deviate in the opposite direction from the MG model predictions. This indicates that variations in the screening criterion, as required for other choices of chameleon theory parameters or for symmetron screening, do not weaken our result. We also show the best fit obtained using a simple average over the best 4 measurements per galaxy (B4). Finally the best fit value using the metallicity correction of Sakai et al (2004) is also shown (Z-corr). The majority of the distance estimates we used did not attempt such a correction. We have not used it in our fiducial best fit since there is a slight correlation of metallicity with level of screening which may introduce correlations with the signal; moreover the goodness of fit for our sample did not improve with the Sakai et al metallicity correction. With a large enough sample of galaxies, one can attempt to create screened and unscreened subsamples that have similar metallicity distributions and thus do a controlled metallicity correction.

We note that cepheid and TRGB distances are calibrated using cepheids with parallaxes and TRGB stars in globular clusters in the Milky Way. Thus we rely on the Milky Way being screened in using them as tests of gravity in unscreened galaxies. This means that, as for other astrophysical/cosmological tests, the constraints we obtain for large values of χ_c (above about 10^{-6}) require an unconventional interpretation of screening to satisfy solar system tests of gravity, such as a significant effect of the mass distribution of the Local Group. On the other hand, if somehow say TRGB stars in the Milky Way were unscreened, thus implying that the TRGB distances in our sample were calibrated with an unscreened luminosity relation, then there would be strong deviations with stellar mass and host galaxy environment (large groups or clusters) that are likely ruled out by current data.

5.1. Constraints on chameleon theories

Figure 5 summarizes our constraints on chameleon theories. In the α_c - χ_c plane, we plot the regions excluded at 68% and 95% confidence with the light and dark shaded regions. We have made some approximations in obtaining this plot, especially in our criteria for screened and unscreened galaxies: we use a fiducial choice $\alpha_c = 1/3$ and vary the subsamples as χ_c varies. The relatively small number of galaxies available is responsible for the jaggedness in the contours. We assume that the environmental screening criterion is not sensitive to the value of α_c directly. While α_c is expected to change the thickness of the shell around screened objects, observable stars are located

well inside the galaxy halo. For our test, the best fit is very robust to the choice of the unscreened sample, as evident from the right panel of Figure 4: essentially we cannot find any selection of galaxy subsamples that correlates with screening and produces a statistically significant deviation from GR.

We have also tested the results shown in Figure 5 with different screening criteria and several methods of estimating systematic errors as described above: the 95% confidence contour is robust to all our tests, while the 68% confidence contour can vary somewhat. A larger galaxy sample and detailed theoretical calculations are required to obtain a more rigorous version of Figure 5.

We summarize our limits for two specific choices of α_c :

- $\alpha_c = 1/3$: Upper limit at 95% confidence: $\chi_c \approx 5 \times 10^{-7}$
- $\alpha_c = 1$: Upper limit at 95% confidence: $\chi_c \approx 1 \times 10^{-7}$.

These limits correspond to a background Compton wavelength of ~ 1 Mpc for the models discussed in the literature (e.g. Schmidt, Vikhlinin and Hu 2009). The very short range of the scalar force implies an extremely limited modification of gravity, i.e. a fine tuned model. The limits on both parameters can be extended further in the near future with additional analysis and forthcoming data on cepheids.

Limits from cosmological tests on the background field value are over two orders of magnitude weaker than the limits obtained here. The cosmological analysis of $f(R)$ gravity (including SN + CMB + ISW + cluster data) done by Schmidt et al (2010) and Lombriser et al (2010) gives the upper limit $\chi_c \approx 10^{-4}$ for $\alpha_c = 1/3$. This limit is also indicated in Figure 5. The constraining power comes mostly from galaxy cluster counts. The constraints on gravity by Reyes et al (2010) that use the test proposed by Zhang et al (2007) do not constrain $\chi_c \sim 10^{-4}$ even at 68% confidence. Cosmological tests have not been used probe values of α_c other than 1/3. While our local astrophysical tests are more powerful for chameleon theories, it is worth noting that more generally any probe of gravity in a distinct regime of length scale and redshift is valuable – in that sense the local tests are complementary to cosmological tests.

5.2. Constraints on symmetron theories

The symmetron screening model has some qualitative similarities to chameleon screening. Hinterbichler and Khoury (2010) showed that solar system tests place constraints on parameters of symmetron cosmology that are analogous to α_c and χ_c . Clampitt, Jain & Khoury (2011) computed the screening profile of galaxy halos of different masses. To translate our results to symmetron models, we use the following relation of our parameters to those of Clampitt et al: $\chi_c \equiv 1/2(M_s/M_{\text{Planck}})^2$ and $\alpha_c = 2g^2$. Solar system tests set the constraint $\chi_c \lesssim 10^{-6}$ or $M_s \lesssim 10^{-3}M_{\text{Planck}}$ for $g = 1$ and a Compton wavelength of ~ 1 Mpc (Hinterbichler & Khoury 2010).

Our upper limit for the fiducial symmetron model described above is $\chi_c \lesssim 3 \times 10^{-7}$. We can extend our results for other values of α_c to the symmetron parameters as well. We do not pursue a more detailed analysis here as it would require the screening condition to be worked out carefully for the symmetron case. We do use the mapping from chameleon to symmetron self-screening described in Clampitt, Jain & Khoury (2012) but the environmental screening needs to be considered more carefully (Joseph Clampitt, private communication).

5.3. Additional Tests of Gravity with Cepheids

We have not considered some additional gravity tests that are possible with distance indicators. These include the following.

- The location of the instability strip and other properties of cepheids (size, luminosity and pulsation amplitude) are affected by modified gravity. With more detailed theoretical predictions, these provide additional tests (Sakstein et al., in preparation).
- Variation of the slope of the $P - L$ relation and its dependence on filter. Since the periods of massive cepheids are affected more strongly, the $P - L$ relation should have a shallower slope for unscreened galaxies. A second effect arises from the steeper slope of the $P - L$ relation in the IR – this means that the inferred distance would be smaller in the IR. We see no hints of a signal with the limited available data, but a useful tests requires significantly more observations with Spitzer and other IR instruments.
- The variation of estimated distance with cepheid mass and temperature and with the degree of screening of the host galaxy. These would require detailed theoretical predictions, a high resolution screening map for different galaxies and a far more detailed analysis of observations than we have performed.

6. Masers and Other Distance Indicators

The comparison of distances from cepheids or TRGB with other methods that rely on self-screened objects can provide useful tests. Distances obtained using Type Ia Supernovae (SN) are likely unaffected by MG for $\chi_c \lesssim 10^{-4}$, while maser distances use a purely geometric method so they are unaffected by MG. We do not attempt to create a screened vs. unscreened galaxy sample in this section since maser and SN distances are not available for sufficient numbers of dwarf galaxies. We rely on the calibration of cepheid or TRGB distances in the Milky Way (taken to be screened either by its own potential or that of the Local Group) and work in the parameter range where these distances are affected by modified gravity. As discussed above, along with other astrophysical or cosmological tests, the logic of pursuing constraints at field values $\chi_c > 10^{-6}$ requires invoking an unconventional source of screening for the solar system.

6.1. Water Masers and the Distance to NGC 4258

Maser distances are inferred by comparing the rotation velocity and proper motion (angular velocity) of water masers in Keplerian motion around supermassive black holes in spiral galaxies. Measurement of the centripetal acceleration provides a second distance estimate. NGC 4258 is a Milky Way sized galaxy at a distance of 7 Mpc. The water masers in this galaxy provide a rotation velocity of the accretion disk in excess of 1,000 km/s at distances on the order of 0.1-0.3 pc from the inferred super-massive black hole of mass $4 \times 10^7 M_{\odot}$. The two distance estimates obtained from the maser data are in excellent agreement – see Herrnstein et al (2005) and Humphreys et al (2008) for recent studies.

A summary of the maser, cepheid and TRGB distance estimates to NGC 4258 following Freedman & Madore (2010) is:

$$\text{NGC4258 Maser : } d = 7.2 \pm 0.2 \text{ Mpc} \tag{15}$$

$$\text{NGC4258 Maser : } d = 7.1 \pm 0.2 \text{ Mpc} \tag{16}$$

$$\text{NGC4258 Cepheid : } d = 7.18 \pm 0.07(\text{statistical}) \text{ Mpc} \tag{17}$$

$$\text{NGC4258 TRGB : } d = 7.18 \pm 0.13 \pm 0.40 \text{ Mpc} \tag{18}$$

There are several caveats to the above tabulation, especially for the cepheid distance which does not include systematic errors, but a full discussion is beyond the scope of this paper (see Benedict et al 2007; di Benedetto et al 2008 and Mager, Madore & Freedman 2008 for recent cepheid distance estimates). We note that the distances agree within estimated errors that are at the few percent level for the maser distances and (allowing for systematics) at the 5-10% level for cepheid and TRGB distances.

The agreement of TRGB and water maser distances probe field values χ_c above 10^{-6} – the precise range probed depends on the value of α_c and the typical mass of the star. Specifically for $\alpha = 1/3$, $\chi_c > 4 \times 10^{-6}$ and a typical star of mass $1.5M_{\odot}$ the TRGB luminosity is smaller by over 20%, corresponding to an inferred distance that is larger by over 10%. Thus given the measurements above, $f(R)$ models with this parameter range are excluded. Note that the maser distance is purely geometric: it is a ratio of velocities or a combination of velocity and accelerations that is independent of the strength of gravity; it is immune to MG effects. Thus higher field values up to the cosmological upper limit of 10^{-4} are also excluded since TRGB distances would change drastically for these values.

The agreement with cepheid distances would probe lower field values but NGC 4258 is a Milky Way sized galaxy, so for lower field values the galaxy would screen the cepheids. One must wait for future observations of masers in smaller galaxies to probe field values below 10^{-6} though it is unclear whether useful maser distances can be found for galaxies with much smaller Newtonian potentials.

6.2. Other Distance Indicators

Type Ia SN are a valuable distance indicator at cosmological distances where cepheid and TRGB methods cannot be applied. The energetics of a Type Ia SN is set by the thermonuclear fusion of Carbon-Oxygen nuclei in the core of the progenitor white dwarf. The emission responsible for the observed optical light curve comes from the expanding shell in which Nickel nuclei decay into Iron and release high energy photons that subsequently thermalize. While the Newtonian potential at the surface of the core is $\sim 10^{-4}$, it is smaller at the distance of the expanding shell. We have not attempted to use supernovae distances as a test here because SN distances are calibrated using cepheid distances for a small number of galaxies with both distance indicators available. With a much larger sample, using a subset of screened galaxies for calibration may make an unscreened subsample available for tests.

Finally, other widely used distance indicators include Tully-Fisher, Fundamental Plane and Surface Brightness Fluctuations. The first two methods rely on the dynamics of stars in disk and elliptical galaxies. The scatter in these methods remains large and their use would require averaging over large numbers of galaxies. We do not pursue these methods here.

7. Discussion

We have used low-redshift distance indicators to carry out tests of scalar-tensor gravity theories. In particular, since different distance indicators operate in gravitational fields of different strengths, their screening behavior varies. A comparison of distance estimates from cepheids, TRGB stars and other distance indicators in nearby dwarf galaxies can provide powerful tests of gravity. The results shown here are applicable to chameleon theories (including all $f(R)$ models) and we have shown rough constraints on symmetron screening as well. Indeed, with the notable exception of theories that use Vainshtein screening, a generic scalar-tensor gravity theory is likely to be constrained by our analysis. Our tests also constrain scalar field couplings to matter that may arise in dark energy, string theory or other scenarios.

Cepheid variables are the least compact of the distance indicators considered here – the amplitude of the surface Newtonian potential is typically $\Phi_N \sim 10^{-7}$ (for TRGB stars the relevant $\Phi_N \gtrsim 10^{-6}$). Thus in unscreened galaxies, cepheids may experience enhanced forces due to the scalar field – this will lower the inferred cepheid distance compared to screened distance indicators. It turns out that the deviation of the inferred distance for cepheids and TRGB stars is in opposite directions, so for field values in which both are unscreened they would show even larger discrepancies.

We have shown that current data is consistent with GR and is inconsistent with chameleon theories over a parameter range that is more than two orders of magnitude below previous astrophysical tests. Figures 4 and 5 show our upper limits for the two parameters: the coupling α_c and

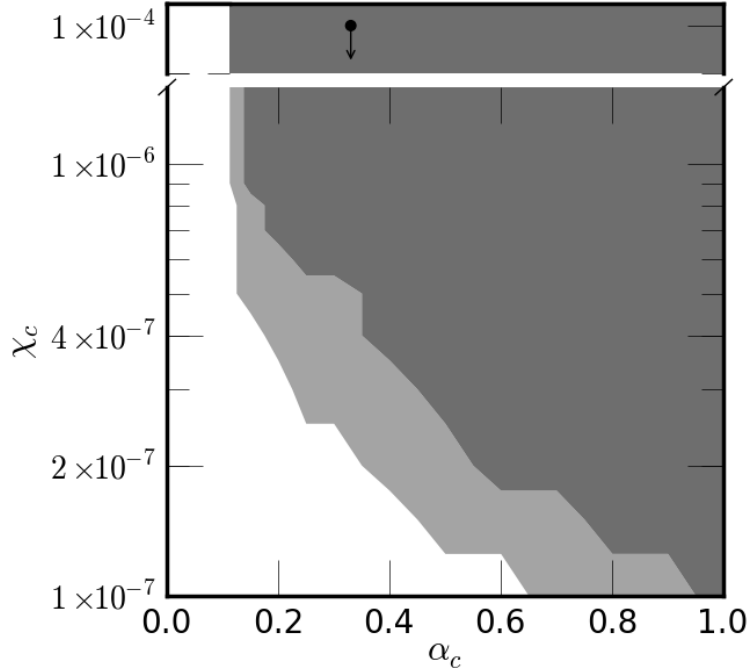


Fig. 5.— Upper limits on the two parameters of chameleon theories: the coupling parameter α_c and the background field value χ_c . The boundaries of the shaded regions show the upper limits at 68% and 95% confidence level. These are obtained using an interpolation of our tests for the two gravity parameters as discussed in the text. The effects of discreteness are due to the small sample of galaxies used. The upper end of the y -axis is extended to $\chi_c = 10^{-4}$ to show the upper limit from cosmological+cluster constraints which was obtained for the $f(R)$ model parameter $f_{R0} \equiv \chi_c$ with $\alpha_c = 1/3$.

the background field value χ_c . For chameleon theories with $\alpha_c = 1/3$ (all $f(R)$ models) the upper limit on χ_c is about 5×10^{-7} at 95% confidence. We show results for values of α_c in the range 0.1 – 1. The upper limit on χ_c drops just below 10^{-7} for $\alpha_c = 1$. The comparison of maser and TRGB distances to NGC 4258 provides an independent test of field values $\chi_c > 2 \times 10^{-6}$.

Cosmological observations so far have probed field values larger than 10^{-4} (Reyes et al 2010; Schmidt, Vikhlinin & Hu 2009; Lombriser et al 2010 and references therein). Thus our limits exceed the combined analysis of cosmological probes by over two orders of magnitude. Our upper limits also exceed solar system and lab tests for some range of chameleon potentials (see e.g. the discussion in Hu & Sawicki 2007 on the comparison of field values in galaxies vs. local tests). With better data on distance indicators, lower values of α_c and χ_c can be tested, though going much below $\alpha_c \approx 0.1$ or $\chi_c \approx 10^{-7}$ will be difficult (due to systematic errors and the self-screening of cepheids, respectively). Observations of nearby dwarf galaxies may probe lower field values, which we explore in a separate study (Vikram et al, 2012).

Thus the primary advantages of local astrophysical tests such as ours are as follows. 1. The signal is stronger – it can be a large fraction of the maximum force modification due to the scalar field. In contrast, the effect on the growth of cosmological fluctuations is typically much smaller. 2. Constraints are more general and translate directly to the two key parameters of the theories. 3. The availability of a control (screened) sample enables robustness to several systematics. 4. There is almost no degeneracy with other cosmological parameters or assumptions. The primary disadvantage is the presence of astrophysical uncertainties: metallicity, galaxy age and stellar population, extinction and so on. However many of these systematics do not affect our tests at lowest order since all our tests are relative, as discussed above (this allows us to carry out tighter tests than say the distance ladder which requires an absolute calibration).

Nevertheless there are three significant sources of uncertainty in our analysis: an incomplete modeling of the theory, systematic errors in the data, and approximations used in determining the screening level of the host galaxies. We have used results reported in the literature on high quality distance measurements, as summarized in Freedman & Madore (2010). We attempted to use multiple weightings of the data as well as different estimates of systematic errors to test for the robustness of our conclusions. Even so we note that the data is inhomogeneous and our understanding of the underlying systematics is limited. Ideally by starting with data on individual cepheids a more careful and complete analysis can be performed.

There are a number of open questions for theoretical work that can sharpen the tests reported here and enable new tests. Predictions for the screening level and effective G in symmetron/dilaton screening scenarios would enable these theories to be tested with the same datasets. Non-adiabatic numerical models of cepheid pulsations are needed to improve on the approximate predictions made here. We have recently learned that the predicted deviations of the period that we have used are close to estimates with such numerical models (which in fact appear to be slightly higher – Philip Chang and Hideyuki Saio, private communication). Several additional tests can be carried out with complete theoretical models that incorporate MG, as discussed in §5.3.

These observational phenomena have been known for a long time – here we have demonstrated a new use for them as tools for testing gravity. Future observations designed with this in mind could obtain more powerful constraints on these theories. Cepheid and TRGB distances to dwarf galaxies out to about 20 Mpc, in a variety of screening environments, are needed to check against relative systematics and improve constraints on gravity. In this respect it would be prudent to carry out new analyses that are designed to be immune to “confirmation bias”. Infrared observations of the cepheid $P - L$ relation can provide a strong new test through the variation of slope of the $P - L$ relation as discussed above. Currently, there is only one galaxy with simultaneous cepheid, TRGB and maser measurements. Maser distances to additional galaxies, especially lower mass galaxies, would strengthen the test described in §6.1. Tests that compare SN and cepheid distances are also worth pursuing.

Acknowledgements: We are extremely grateful to Bill Paxton for developing and making public

the software package MESA and answering our numerous questions. We are very grateful to Anna Cabre, Joseph Clampitt, Anne Davis, Lam Hui, Mike Jarvis, Eugene Lim, Hideyuki Saio and especially Philip Chang for discussions and related collaborative studies. We acknowledge helpful discussions with Gary Bernstein, Wayne Hu, Justin Khoury, Kazuya Koyama, Adam Lidz, Raquel Ribeiro, Abhi Saha, Fabian Schmidt, Mark Trodden, Amol Upadhye, Jake VanderPlas and Gongbo Zhao. BJ is partially supported by NSF grant AST-0908027. JS is supported by the STFC.

A. Scalar-Tensor Modifications of Gravity with Screening mechanisms

As pointed out in the introduction, any viable theory of modified gravity must recover our solar system tests of GR and so we require a screening mechanism in order to have non-trivial modifications to the dynamics on large (cosmological) scales. Such screening mechanisms can arise through the scalar-tensor action

$$S = \int d^4x \sqrt{g} \left[\frac{m_{\text{pl}}^2}{2} R - \frac{1}{2} \nabla_\mu \phi \nabla^\mu \phi - V(\phi) \right] + S_{\text{m}}[\Psi_i; \tilde{g}_{\mu\nu}], \quad (\text{A1})$$

where S_{m} denotes the action for the matter fields and Ψ_i represent all matter species in the system. This action looks a lot like the usual action for GR except that the matter fields are not coupled to gravity via the metric but instead via the conformally scaled, *Jordan Frame* metric $\tilde{g}_{\mu\nu} = A^2(\phi)g_{\mu\nu}$. Here $A(\phi)$ is an arbitrary function of a new scalar ϕ which is known as the *coupling function*. This action is known as the *Einstein frame* action since the scalar field ϕ is coupled non-minimally to the Ricci scalar. One could instead conformally transform to the Jordan frame where the fields would couple minimally to gravity but now the scalar is coupled non-minimally to gravity via the Ricci scalar $A^{-2}(\phi)R$. In this work we shall work exclusively in the Einstein frame since this is where all of our physical tests of GR lie. In this frame, matter fields follow geodesics of the $\tilde{g}_{\mu\nu}$ whilst observers in Einstein frame travel along geodesics of $g_{\mu\nu}$ and so these observers see an additional or *fifth* force given (per unit mass) by (see Waterhouse 2006)

$$F_\phi = \frac{\beta(\phi)}{m_{\text{pl}}} \nabla \phi \quad \text{where} \quad \beta(\phi) \equiv m_{\text{pl}} \frac{d \ln A}{d\phi} \quad (\text{A2})$$

is known as the *coupling*. There are two methods by which the scalar-tensor screening mechanism can act. Either the mass of the scalar is very large (the field gradient is small) so that the force is Yukawa suppressed or the coupling $\beta(\phi)$ is very small and the force is negligible. The first mechanism is utilised by the chameleon mechanism (Khoury & Weltman 2004), whereas the second is utilised by the symmetron (Hinterbichler & Khoury 2010) and the environmentally dependent dilaton (Brax et al. 2010)

In this section we shall first describe how these conditions can be achieved in general in the neighborhood of our solar system before elucidating this further with some common examples.

A.1. The General Mechanism

Varying the action with respect to the field ϕ results in the equation of motion

$$\square\phi = V_{,\phi} - T_m(\ln A)_{,\phi} \quad (\text{A3})$$

where T is the trace of the energy-momentum tensor in the Einstein frame. In standard GR we have $T_m = -\rho$ where ρ is the matter density, however, due to the non-minimal coupling to the scalar field it is the Jordan frame and not the Einstein frame density that is covariantly conserved. It can be shown (Waterhouse T.-P.) that the quantity $A^3\rho$ satisfies the non-relativistic continuity equation and so, taking this as our matter density from here on, equation A3 defines a density dependent effective potential for ϕ

$$V_{\text{eff}}(\phi) = V(\phi) + \rho A(\phi). \quad (\text{A4})$$

It is this density dependence of the effective potential that is responsible for the screening mechanism. Consider a body of high density (e.g. a star or galaxy) emersed inside a much larger medium of smaller density (the universe) and suppose that the effective potential has a minimum. The minimum of the effective potential will lie at different field values depending on the density and so the field will try to minimise this potential inside both media. The outer medium is much larger than the high density medium and so the field will always reach its minimum at asymptotically large distances from the smaller body. Theories with screening mechanisms have the property that either the coupling β at the minimum becomes negligible at high densities or the mass of oscillations about said minimum is very large. Hence if the field can minimise its effective potential effectively inside the high density body then the fifth force will be screened, if this is not possible then the body will be unscreened and the Newtonian force law will receive order one corrections.

To see this more quantitatively, consider a spherically symmetric body of density ρ_b immersed in a much larger medium with density ρ_c with $\rho_b \gg \rho_c$. In the theories of interest to us we have $\phi_b \ll \phi_c$. Inside the medium the field minimises its effective potential at field value ϕ_c and inside the body the field may or may not reach its value which minimises the effective potential, ϕ_b . If the object is static i.e. on changes occur on a time-scale much smaller than the time-scale for cosmological evolution of the field then equation A3 becomes

$$\nabla^2\phi = V(\phi)_{,\phi} + \rho A(\phi)_{,\phi}. \quad (\text{A5})$$

Suppose that the field has reached ϕ_b at $r = 0$. In this case we have $V(\phi)_{,\phi} \approx -\rho A(\phi)_{,\phi}$ and equation A5 has no source term and $\phi \approx \phi_b$. In this case there is no field gradient and the fifth force is not present. Of course the field must asymptote to ϕ_c away from the body and so there must be some radius r_s at which this approximation no longer holds and the source terms become important. In this region the field will possess some gradient and approach its asymptotic values and so we expect order one fifth forces. r_s is hence known as the *screening radius*; the region interior to this is screened whilst the exterior region is unscreened. In the unscreened region, the field is

a small perturbation about its cosmological value and so we can linearise equation A5 by setting $\phi = \phi_c + \delta\phi$ to find

$$\nabla^2 \delta\phi \approx m_c^2 \delta\phi + \frac{\beta(\phi_c)}{m_{\text{pl}}} \delta\rho \quad (\text{A6})$$

where $\delta\rho = \rho_b - \rho_c$ and $m_c^2 = d^2V(\phi)/d\phi^2$ is the mass of the field in the cosmological vacuum. On length scales $R \ll 1/m_c$ i.e. on those far less than the range of the fifth force in vacuum, we can neglect the first term and the second term can be related to the Newtonian potential via the Poisson equation $\nabla^2 \Phi_{\text{N}} = 4\pi G \delta\rho$. Integrating this twice gives the field in the unscreened region

$$\delta\phi(r) \approx -\phi_c + 2\beta_c m_{\text{pl}} \left[\Phi_{\text{N}}(r) - \Phi_{\text{N}}(r_s) + r_s^2 \Phi'_{\text{N}}(r_s) \left(\frac{1}{r} - \frac{1}{r_s} \right) \right] \quad r_s < r \ll m_c^{-1} \quad (\text{A7})$$

where we have used the fact that $\phi_b \ll \phi_c$ to set the boundary condition $\delta\phi(r_s) \approx -\phi_c$. Using this in equation A2, we find the total force per unit mass (Newtonian plus fifth) in the unscreened region is

$$F = F_\phi + F_{\text{N}} = \frac{G(r)M(r)}{r^2} \quad \text{where} \quad G(r) = G \left[1 + \alpha_c \left(1 - \frac{M(r_s)}{M(r)} \right) \right] \quad (\text{A8})$$

where $\alpha_c \equiv 2\beta_c^2$ and $M(r)$ is the mass contained inside a shell of radius r . Taking the limit as $r \rightarrow \infty$ in equation A7 gives us an implicit relation for the screening radius in terms of the Newtonian potential

$$\chi_c \equiv \frac{\phi_c}{2m_{\text{pl}}\beta(\phi_c)} = -\Phi(r_s) - r_s \Phi'_{\text{N}}(r_s). \quad (\text{A9})$$

The quantity χ_c controls the ability of objects to self screen. Clearly if the surface Newtonian potential $\Phi_{\text{N}}(R) < \chi_c$ then equation A9 can never be satisfied and the body is completely unscreened ($r_s = 0$) whilst if the converse is true then the body will be at least partially screened. If the body is completely unscreened then equation A8 gives us an order one enhancement of the Newtonian force by a factor $(1 + \alpha_c)$.

A.2. Chameleon Screening

Any theory where the coupling function $A(\phi)$ is a monotonically increasing function of ϕ falls into the class of *chameleon* theories. The chameleon mechanism operates by exploiting the density dependence of the mass of the scalar field; in high density environments the mass is large and the force is very short ranged (Yukawa suppressed) whilst in low density (cosmological) environments the force range can be very large. It is this mass blending in with its environment that gives rise to its name. The large mass inside the body means that when the field can reach its minimum at the centre (i.e. the screened case) it is frozen there over much of the body's interior and varies only in a very thin shell near the surface in order to reach its cosmological value. This has the effect that the force exterior to the object receives contributions from flux lines within this thin shell only and not the entire body and is hence suppressed by a small factor $\Delta R/R \approx \phi_c/6m_{\text{pl}}\beta_c\Phi_{\text{N}}(R)$. This phenomena is known as the *thin shell effect*.

In the original models (Khoury & Weltman 2004) the potential was taken to be of the run-away form

$$V(\phi) = \lambda \frac{M^{4+n}}{\phi^n} \quad \text{with } n > 0 \quad (\text{A10})$$

however it was pointed out that power law potentials can also act as chameleons (Gubser & Khoury (2005); Brax et al (2010a) and Mota & Winther (2011)). Indeed, Mota & Shaw (2006) have investigated the constraints that current fifth-force searches place on these models and have found that both $n > 0$ and $n < 0$ potentials are viable. The fiducial coupling considered by Khoury & Weltman (2004) is $A(\phi) = \exp(\beta\phi/m_{\text{pl}})$ where β is constant and $\mathcal{O}(1)$ although it has been shown that field dependent couplings are perfectly viable (Brax et al. 2010a; Mota & Winther 2011). With this coupling the fifth force is of gravitational strength however, fifth force searches do not in fact rule out very strong couplings to matter Mota & Shaw (2006) and $\beta_c/m_{\text{pl}} \leq 10^9$ are viable ⁷.

The chameleon cosmology is constrained to behave almost identically to Λ CDM due to BBN constraints. The coupling of the chameleon to matter gives a field dependent mass to the standard model particles. The variation of nucleon masses between BBN today is constrained heavily and this enforces the condition that the chameleon remain in its minimum over the entire cosmic history from BBN until the present. This then requires that the minimum of the potential is an attractor i.e. that $m_c \gg H^2$ throughout the cosmic history. It has been shown that a wide variety of models have this feature and can hence act as dark energy and reproduce the current cosmic expansion (Brax et al. 2003; Gannouji et al. 2010; Mota et al. 2011).

A.3. Symmetron Screening

Consider an effective potential which possesses some symmetry that acts on the field. If the symmetry is broken then ϕ will acquire a non-zero vacuum expectation value (VEV) whereas if the symmetry is unbroken the field VEV is identically zero. Symmetron screening (Khoury & Hinterbichler 2010) relies on symmetry restoration in high density environments and includes a coupling β that becomes zero at field values where the symmetry is restored. In low density environments the symmetry is broken and order unity fifth forces are present, whereas in the vicinity of our solar system the symmetry is restored and fifth forces are negligible thereby satisfying local constraints.

The fiducial model uses the effective potential and coupling functions, defined as for chameleon theories above, given by

$$V(\phi) = -\frac{1}{2}\mu^2\phi^2 + \frac{\lambda}{4!}\phi^4; \quad A(\phi) = 1 + \frac{\phi^2}{2M^2} \quad (\text{A11})$$

⁷This essentially stems from the fact that the Eöt-Wash experiment does not search for fifth forces directly but rather searches for deviations from the inverse square law of Newtonian gravity. At large couplings, the fifth force is a simple rescaling of the gravitational constant and hence the Eöt-Wash experiment is insensitive to it.

such that the effective potential is \mathbb{Z}_2 symmetric with the coefficient of the quadratic term being density dependent

$$V_{\text{eff}}(\phi) = \frac{1}{2} \left(\frac{\rho}{M^2} - \mu^2 \right) \phi^2 + \frac{\lambda}{4!} \phi^4. \quad (\text{A12})$$

In low density environments this coefficient is negative and the symmetry is spontaneously broken while in high density environments it is restored and the field moves to zero VEV. The coupling is given at leading order by $\beta \propto \phi$ and so the force enhancement is negligible in high density regions. The parameters in the model are chosen such that cosmic acceleration begins around the current epoch – this has the result that the range of the force on cosmological scales is $\lesssim 1$ Mpc, so a cosmological constant is needed in order to drive the cosmic acceleration (Hinterbichler et al. 2011; Davis et al 2011b). In fact this choice of potential and coupling function should be thought of as a leading order approximation and any more general effective potential that has a density dependent quadratic (or possibly higher order if quadratic terms are absent all together) term will exhibit such a screening mechanism provided that the minimum is symmetry breaking at zero density. Hinterbichler et al. (2011) consider such a potential, but find that this does not remove the need for a cosmological constant. One should note that the symmetry is not in fact required for this mechanism to operate. Any general effective potential that admits one minimum ϕ_0 at zero density, which is replaced by a different minimum at ϕ_ρ in larger densities with the property that $\beta(\phi_\rho) \ll 1$ will, in theory, possess such a screening mechanism.

A.4. The Environmentally Dependent Dilaton

The environmentally dependent dilaton (Brax et al. 2010b) arises in the four dimensional low energy effective action of string theory in the strong coupling limit. In the Einstein frame, the action is given by

$$S = \int d^4x \sqrt{g} \left[\frac{m_{\text{pl}}^2}{2} R - k^2(\phi) \nabla_\mu \phi \nabla^\mu \phi - V(\phi) \right] + S_{\text{m}}[\Psi_i; \tilde{g}_{\mu\nu}] \quad (\text{A13})$$

where

$$k^2(\phi) = \frac{1}{\lambda^2} + 3\beta^2(\phi) \quad \text{and} \quad V(\phi) = V_0 A^4(\phi) e^{-\frac{\phi}{m_{\text{pl}}}} \quad (\text{A14})$$

with $\lambda \sim \mathcal{O}(1) - \mathcal{O}(\gg 1)$ In this model, the coupling function is not known explicitly but is assumed to have a minimum at some ϕ_0 and so is taken to be (near the minimum) $A(\phi) = 1 + A_2/2(\phi - \phi_0)^2$ where $A_2 \gg 1$ in order to satisfy local constraints. The non-canonical kinetic term has two effects. Firstly, the canonically normalised field φ feels an effective potential

$$V_{\text{eff}}(\varphi) = V_0 A^4(\phi) e^{-\frac{\phi}{m_{\text{pl}}}} + \rho A(\phi) \quad \text{where} \quad \phi = \phi(\varphi) \quad (\text{A15})$$

and secondly, the usual fifth-force law is modified to

$$F_\phi = \frac{\beta^2(\phi)}{k^2(\phi)} F_{\text{N}} \quad (\text{A16})$$

in unscreened regions (note that $k^2 = 1/2$ for canonically normalised fields). Minimising the effective potential, one finds the coupling and force enhancement as a function of density at the minimum

$$\beta(\phi_{\min}) = A_2(\phi_{\min} - \phi_0) = \frac{V_0 e^{-\frac{\phi_{\min}}{m_{\text{pl}}}}}{\rho + 4V_0 e^{-\frac{\phi_{\min}}{m_{\text{pl}}}}}; \quad \alpha(\phi_{\min}) = \frac{\lambda^2 \beta^2(\phi_{\min})}{3\lambda^2 \beta^2(\phi_{\min}) + 1}. \quad (\text{A17})$$

In this case high density environments push ϕ to its value that minimizes the coupling function and $\beta \rightarrow 0$, thus screening the force enhancement (note that minimising A is precisely the condition that the fifth-force vanish). The condition for efficient screening, $A_2 \gg 1$ is precisely the condition that the cosmological minimum be an attractor and so the environmentally dependent dilaton, like the chameleon can act as dark energy without the need for a cosmological constant.

Unlike the chameleon (where the coupling is approximately constant) and the symmetron (whose VEV is only weakly dependent on the density), the dilaton's coupling is very sensitive to the cosmological parameters and this allows the fifth force enhancement today to be placed somewhere in the range $0.045 \leq \alpha \leq 1/3$.

B. TRGB Distances in Modified Gravity

In this section we briefly show how inferred TRGB distances can be greater than the true value if the core of the star is unscreened. The luminosity of a star ascending the red giant branch is due entirely to a very thin hydrogen burning shell just above the helium core. The triple alpha process ignites in a process known as the helium flash at temperatures $T \sim 10^8$ K and so for temperatures below this the core has no source of outward pressure and contracts. As the star climbs further the radius of the core decreases whilst the mass increases due to fresh helium being deposited by the shell. This results in a gradual increase until the core temperature is high enough to begin helium burning, at which point the star moves to the left in the H-R diagram. In GR, this sudden jump to the left occurs at a fixed luminosity, however, as we shall see below, this luminosity at the tip is lower in MG, provided that the core is unscreened.

Treating the core as a solid sphere of fixed temperature T_c , mass M_c and luminosity L , the hydrogen burning shell is incredibly thin and can be treated as having constant mass and luminosity. In this case, the shell pressure and temperature is given by the hydrostatic equilibrium and radiative transfer equations,

$$\frac{dP}{dr} = -\frac{GM_c \rho(r)}{r^2}; \quad \frac{dT^4}{dr} = \frac{3}{4a} \frac{\kappa(r) \rho(r) L}{4\pi r^2} \quad (\text{B1})$$

which can be used to find

$$P \propto \frac{GM_c T^4}{L}, \quad (\text{B2})$$

where the opacity in the hydrogen shell is due mainly to electron scattering and so we have taken it to be constant. The pressure in the shell is due mainly to the gas and so we ignore radiation

pressure and take the equation of state to be that of an ideal gas, $P \propto \rho T$. Using this and equation B2 in the radiative transfer equation we find

$$T(r) \propto \frac{GM_c}{r}, \quad (\text{B3})$$

where the integration constant is negligible near the base of the shell. Next, we can estimate the luminosity given an energy generation rate per unit mass $\epsilon \propto \rho(r)T(r)^\nu$

$$L = \int 4\pi r^2 \rho(r) \epsilon(r) dr. \quad (\text{B4})$$

For temperatures above 10^7 K, which is the case in the shell, hydrogen burning proceeds mainly via the CNO cycle and so $\nu = 15$. Using the equation of state and the results above in equation B4 one finds

$$L \propto \frac{G^{\frac{8}{3}} M_c^{7.7}}{R_c^6}. \quad (\text{B5})$$

Now suppose that the core becomes unscreened so that $G(r) \approx G(1 + \alpha_e)$ where α_e is the effective value of α_c in the core given by equation A8. The He flash occurs at a fixed temperature, independent of MG, and so if we set $\xi = M_c/R_c$ at the point when $T_c = 10^8$ K then we have $\xi_{\text{MG}}/\xi_{\text{GR}} = (1 + \alpha_e)^{-1} < 1$. The ratio of the core mass to the core radius at the He flash in MG is then lower than that in GR. In general, this does not tell us anything about the core mass and radius individually, however, in practice one finds that the core radius is the same in both cases (this is borne out by MESA simulations) and so this is a relation between the core masses at fixed temperature. Using equation B5 we then have

$$\frac{L_{\text{MG}}}{L_{\text{GR}}} = \frac{1}{(1 + \alpha_e)^{\frac{15}{3}}} \quad (\text{B6})$$

and hence the peak luminosity is lower in MG, contrary to what one would expect if the argument that radii are generally smaller in MG is followed.

To infer distances using the TRGB method, one observes the flux ($\propto L/d^2$) and uses the (nearly) universal luminosity at the tip. If the star is indeed unscreened then its luminosity in MG is lower than the universal value assumed, so one would over-estimate the distance.

C. Data

Table 4: The galaxies used in the $P - L$ relation and their references. The second column labeled N gives the number of cepheids observed for each galaxy. Names that end with * are galaxies with unacceptably large dispersion in P-L relation.

Name	N	Reference
NGC300	117	Pietrzyński et al. (2002)
NGC5253	5	Saha et al (2006)
IC4182	13	Saha et al (2006)
NGC925	79	Silbermann et al (1996)
NGC2541	28	Ferrarese et al. (1998)
NGC3319	28	Sakai et al. (1999)
NGC1326A	17	Prosser et al. (1999)
NGC 2090	34	Phelpset al. (1998)
NGC 3031	25	Freedman et al. (1994)
NGC 3198	52	Kelson et al. (1999)
NGC 3351*	49	Graham et al. (1997)
NGC 3621*	69	Rawson et al. (1997)
NGC 4321*	52	Ferrarese et al. (1996)
NGC 4414*	9	Turner et al. (1998)
NGC 4535	50	Macri et al. (1999)
NGC 4548*	24	Graham et al. (1999)
NGC 4725	20	Gibson et al. (1999)
NGC 5457	29	Kelson et al. (1996)
NGC 7331	13	Hughes et al. (1998)

Table 5: Cepheid and TRGB based distances to the galaxies used in the paper. The final column gives the screening for $\phi = 4 \times 10^{-7}$ as follows: 0: Unscreened, 1: environmentally screened, 2: self-screened.

Name	Cepheid D(Mpc)	TRGB D (Mpc)	Screening
DDO 069	0.71 ± 0.01	0.78 ± 0.03	0
NGC 3109	1.15 ± 0.03	1.27 ± 0.02	0
DDO 216	1.27 ± 0.27	0.97 ± 0.03	0
Sextans A	1.31 ± 0.03	1.38 ± 0.03	0
Sextans B	1.49 ± 0.11	1.34 ± 0.02	0
GR8	1.80 ± 0.06	2.19 ± 0.15	0
NGC 0300	2.03 ± 0.05	1.95 ± 0.06	0
NGC 2403	3.20 ± 0.15	3.18 ± 0.35	0
NGC 2366	3.28 ± 0.30	3.19 ± 0.41	0
NGC 5253	3.43 ± 0.08	3.77 ± 0.19	0
NGC 4395	4.45 ± 0.37	4.61 ± 0.62	0
IC 4182	4.68 ± 0.04	4.47 ± 0.12	0
NGC 3621	7.17 ± 0.06	7.45 ± 0.38	0
SMC	0.06 ± 0.00	0.06 ± 0.00	1
NGC 6822	0.51 ± 0.03	0.48 ± 0.01	1
IC 1613	0.69 ± 0.01	0.72 ± 0.01	1
IC 0010	0.72 ± 0.05	0.50 ± 0.04	1
M33	0.90 ± 0.02	0.88 ± 0.02	1
WLM	0.95 ± 0.05	0.91 ± 0.02	1
M31	0.86 ± 0.02	0.78 ± 0.02	2
NGC 5128	3.44 ± 0.19	3.73 ± 0.24	2
M81	3.84 ± 0.06	4.04 ± 0.22	2
M83	5.01 ± 0.23	4.51 ± 0.31	2
M101	7.13 ± 0.14	7.66 ± 0.39	2
M106	8.41 ± 0.07	7.31 ± 0.30	2

REFERENCES

- Alibert, Y., Baraffe, I., Hauschildt, P., & Allard, F. 1999, *A&A*, 344, 551
- di Benedetto G. P., 2008, *MNRAS*, 390, 1762
- Benedict GF, McArthur BE, Feast MW, Barnes TG, Harrison TE, et al. 2007, *ApJ*, 79, 453
- Bono, G., Caputo, F., & Marconi, M. 1998, *ApJ*, 497, L43
- Bono, G., & Marconi, M. 1997, *MNRAS*, 290, 353
- Bono, G., Marconi, M., & Stellingwerf, R. F. 1999, *ApJS*, 122, 167
- Bono, G., Caputo, F., Castellani, V. & Marconi, M. 1999, *ApJ*, 512, 711 (Bono et al 1999b)
- Brax, P., Van de Bruck, C., Davis, A.C., Khoury J., Weltman, A. 2004, *Phys. Rev. D*, 70, 123518
- Brax, P., Van de Bruck, C., Mota, D.F., Nunes, N.J. & Winther, H.A. 2010a, *Phys. Rev. D*, 82, 083503
- Brax, P., Van de Bruck C., Davis, A.C. & Shaw, D.J. 2010b, *Phys. Rev. D*, 82, 063519
- Brax, P., Burrage, C. & Davis, A.C. 2011, *JCAP*, 1109, 020
- Cabre, A., Vikram, V., Zhao, G., Jain, B. 2012, in preparation
- Carroll, Bradley W., & Ostlie, Dale A. 2006, "An introduction to modern astrophysics and cosmology"
- Carroll, S. M., Duvvuri, V., Trodden, M. & Turner, M. S. 2004, *Phys. Rev. D*, 70, 043528
- Chan, K. C., & Scoccimarro, R. 2009, *PRD*, 80, 104005
- Chang, P. & Hui, L. 2011, *ApJ*, 732, 25
- Chiosi, C., Wood, P. R., & Capitanio, N. 1993, *ApJS*, 86, 541
- Clampitt, J. Jain, B. & Khoury, J. 2011, arXiv:1110.2177
- Cox, J. P., 1980, "Theory of Stellar Pulsation,"
- Da Costa, G. S., & Armandroff, T. E. 1990, *AJ*, 100, 162
- Davis, A., Lim, E. A., Sakstein, J., Shaw, D, 2011a, arXiv:1102.5278
- Davis, A.C., Li, B., Mota, D.F. & Winther, H.A. 2011b, *Astrophys.J*, 748, 61
- Decca, R.S., Lopez, D., Fischbach, E., & Krause, D.E. 2003 *Phys. Rev. Lett.*, 91, 050402

- Epstein, I. 1950, ApJ, 112, 6
- Ferrarese, L. et al., 1996, ApJ, 464, 568
- Ferrarese, L., et al., 1998, ApJ, 507, 655
- Freedman W.L., et al., 1994, ApJ, 427, 628
- Freedman W.L., et al., 2001, ApJ, 553, 47
- Freedman W.L., Madore, B. F., 2010, Ann. Rev. Astro. Astrophys., 48, 673
- Gannouji, R., Moraes B., Mota, D.F., Polarski D., Tsujikawa, S. & Winther, H.A. 2010, Phys. Rev. D, 82, 124006
- Graham, J.A. et al. 1997. ApJ, 477, 535.
- Graham, J.A. et al., 1999 ApJ, 516, 626
- Gibson, B.K. et al., 1999, ApJ, 512, 48
- Herrnstein, J., et al. 2005, ApJ, 629, 719
- Hinterbichler, K., Khoury, J., 2010, Phys. Rev. Lett., 104, 231301
- Hinterbichler, K., Khoury, J., Levy, A. & Matas, A. 2011, Phys. Rev. D, 84, 103521
- Hu W., Sawicki I., 2007, Phys. Rev. D, 76, 064004
- Hui, L., Nicolis, A., & Stubbs, C. W. 2009, Phys. Rev. D, 80, 104002
- Hui, L. & Nicolis, A. 2012, arXiv:1201.1508
- Hughes, S.M.G., et al., 1998, ApJ, 501, 32
- Humphreys, E., et al. 2008, ApJ, 672, 800
- Jain B., Khoury J., 2010, Ann. Phys., 325, 1479
- Jain, B. & VanderPlas, J. 2011, J. Cosmology Astropart. Phys., 10, 32
- Kapner, D.J., Cook, T.S., Adelberger, E.G., Gundlach, J.H., Heckel, B.R., Hoyle, C.D. and Swanson, H.E. 2007, Phys. Rev. Lett., 98, 021101
- Kelson, D.D. et al., 1996, ApJ, 463, 26
- Kelson, D.D., et al., 1999, 514, 614
- Khoury J., Weltman A., 2004, Phys. Rev. D, 69, 044026

- Lamoreaux, S.K. 1997, *Phys. Rev. Lett.*, 78, 5
- Lee, M. G., Freedman, W. L. & Madore, B. F. 1993, 417, 553
- Lombriser, L., Slosar, A., Seljak, U., & Hu, W. 2010, arXiv:1003.3009
- Lombriser, L., Koyama, K. Zhao, G-B. & Li, B. 2012, arXiv:1203.5125
- Macri, L. et al., 1999, *ApJ*, 521, 155
- Mager V., Madore B., Freedman, W. 2008, *ApJ*, 689, 721
- Méndez, B., Davis, M., Moustakas, J., Newman, J., Madore, B. F., & Freedman, W. L. 2002, *AJ*, 124, 213
- Mota, D.F. & Shaw, D.J. 2006, *Phys. Rev. D*, 75, 063501
- Mota, D.F. & Winther, H.A. 2011, *Astrophys.J*, 733, 7
- Mould J.R. et al., 2000, *ApJ*, 528, 655
- Paxton, B., Bildsten, L., Dotter, A., Herwig, F., Lesaffre, P & Timmes,F. 2011 *ApJS*, 192, 3
- Phelps, R.L. et al., 1998, *ApJ*, 500, 763
- Pietrzyński, G., Gieren, W., Fouqué, P., & Pont, F., 2002, *AJ*, 123, 789
- Prosser, C.F., et al., 1999, *ApJ*, 525, 80
- Rawson, D.M. et al., 1997, *ApJ*, 490, 517
- Reyes, R. et al., 2010, *Nature*, 464, 256
- Saha, A., et al, 2006, *ApJS*, 165, 108
- Sakstein et al. 2011, in preparation
- Sasselov, D., et al, 1997, *A&A*, 324, 471
- Sakai, S., et al. 1999, *ApJ*, 523, 540
- Sakai, S., et al. 2004, *ApJ*, 608, 42
- Schmidt, F., Vikhlinin, A., & Hu, W. 2009, *Phys.Rev. D*, 80, 083505
- Schmidt, F. 2010, *Phys. Rev. D*, 81, 103002
- Silbermann, N.A. et al, 1996, *ApJ*, 470, 1
- Silvestri, A. & Trodden, M., 2009, *Rept. Prog. Phys.*, 72, 096901

- Starobinsky, A. A., 2007, JETP Lett. 86, 157
- Stetson, P. B. 1987, PASP, 99, 191
- Stetson, P. B. 1994, PASP, 106, 250
- Turner, A. et al., 1998, ApJ, 505, 207
- Vainshtein, A. I., 1972, Phys. Lett. B, 39, 393
- Vikram, V, Cabre, A., Jain, B. & VanderPlas, J., 2012, in preparation
- Waterhouse, T.-P. 2006, astro-ph/0611816
- Weinberg, S. 1965, Phys. Rev. B, 4, 138
- C. M. Will, Living Rev. Rel., 2006, 9, 3
- Zhao, G.-B., Li, B., & Koyama, K. 2011, PRL, 107, 071303